Thin-Film Stabilization of Metastable Phases in the $Sm_{1-x}Sr_xCuO_y$ System

A. Gupta

IBM Research Division, Thomas J. Watson Research Center, Yorktown Heights, New York 10598-0218

B. Mercey, H. Hervieu, and B. Raveau

Laboratoire Crismat, CNRS 1318-ISMRA/Université de Caen, Bd du Maréchal Juin, 14050 Caen Cedex, France

Received February 28, 1994®

The pulsed laser deposition (PLD) technique has been utilized for thin film synthesis of new metastable phases in the $Sm_{1-x}Sr_xCuO_y$ ($y = 2.5-0.5x + \delta$) system. The films are grown epitaxially on (100)-oriented $SrTiO_3$ substrates in a low-pressure oxygen ambient with *in situ* monitoring using reflection high-energy electron diffraction (RHEED). X-ray diffraction and transmission electron microscopy are used for structural characterization of the films. Although the synthesis of $SmCuO_{3-\delta}$—the structural analogue of the defect perovskites $LaCuO_{3-\delta}$ ($0 \le \delta \le 0.5$)—have not been successful, perovskite-type phases have been stabilized with Sr substitution over a relatively wide composition range ($0.4 \le x \le 0.66$). With further increase in the Sr content, an ordered $2\sqrt{2}a_p \times 2\sqrt{2}a_p \times a_p$ structure with mixed copper valence has been synthesized for $x \sim 0.75$. Finally, for terminal Sr concentrations ($x \ge 0.9$), the doped infinite-layer-type $SrCuO_2$ phases are obtained. The transport properties of the $Sm_{1-x}Sr_xCuO_y$ films are sensitive to the oxygen concentration used during deposition and subsequent cooldown. For films cooled in 760 Torr of O_2, a systematic decrease in the resistivity is observed as a function of Sr content, with the lowest resistivity and metallic temperature dependence being observed for the ordered structure. However, films with higher Sr concentrations, with the infinite-layer structure, exhibit relatively high resistivity under these annealing conditions. A significant decrease in the resistivity, along with semimetallic temperature dependence, is observed for these (Sm-doped) films when they are vacuum annealed prior to cooldown. No evidence of superconductivity has been detected in any of the $Sm_{1-x}Sr_xCuO_y$ films down to 5 K.

Introduction

In recent years the pulsed laser deposition (PLD) technique has rapidly gained acceptance as a simple and versatile tool for the growth of thin films.[1] In particular, it has found extensive usage for the deposition of films or multicomponent phases like the high-T_c cuprate superconductors and ferroelectric oxide materials. There is also a growing realization that the nonequilibrium conditions prevalent during PLD growth can be gainfully exploited for the pseudomorphic stabilization of novel metastable and artificially structured materials, which would normally be difficult or impossible to obtain by conventional solid-state synthetic methods. For example, films of the tetragonal infinite-layer compounds, $Ca_{1-x}Sr_xCuO_2$ ($0.18 \le x \le 1$), have been grown at low temperatures using PLD.[2] Although these compounds have been prepared in the bulk, they require extreme temperature and pressure conditions for synthesis.[3] More recently, films of the infinite-layer compound with the end member composition, $CaCuO_2$, have also been stabilized by utilizing an epitaxial layer of $SrCuO_2$ as a chemical template.[4] The bulk synthesis of this highly metastable phase has not been successful, even at high pressures.

Thin film stabilization of perovskite-type compounds, involving rare-earth substitutions of the infinite-layer phase materials, represents a natural extension to the search for other metastable cuprates which may exhibit novel structural and electronic properties, including superconductivity.[5] Recently, a number of such compounds have been isolated in the bulk, primarily in the $La_{1-x}Sr_xCuO_y$ system using high-pressure synthesis. These include the rare-earth (RE = Nd, La, Sm, Gd) doped infinite-layer phase compounds, $Sr_{1-x}RE_xCuO_2$ ($x \le 0.1$), which exhibit n-type superconductivity with T_c's $\sim$ 40 K.[6] Some defect perovskite compounds, with ordered oxygen vacancies, have also been isolated for higher rare-

® Abstract published in *Advance ACS Abstracts*, June 15, 1994.

(1) For example, see: *Laser Ablation for Materials Synthesis*; Paine, D. C., Bravman, J. C., Eds.; Materials Research Society: Pittsburgh, PA, 1990.

(2) (a) Norton, D. P.; Chakoumakos, B. C.; Budai, J. D.; Lowndes, D. H. *Appl. Phys. Lett.* **1993**, *62*, 1679–1681. (b) Niu, C.; Lieber, C. M. *J. Am. Chem. Soc.* **1993**, *115*, 137–144. (c) Li, X.; Kawai, T.; Kawai, S. *Jpn. J. Appl. Phys.* **1992**, *31*, L934–L937.

(3) (a) Takano, M.; Takeda, Y.; Okada, H.; Miyamoto, M.; Kusaka, T. *Physica C* **1989**, *159*, 375–378. (b) Siegrist, T.; Zahurak, S. M.; Murphy, D. W.; Roth, R. S. *Nature* **1988**, *334*, 231–232.

(4) Gupta, A.; Hussey, B. W.; Shaw, T. M.; Guloy, A. M.; Chern, M. Y.; Saraf, R. F.; Scott, B. A. *J. Solid State Chem.*, in press.

(5) Raveau, B.; Michel, C.; Hervieu, M.; Groult, D. *Crystal Chemistry of High-T_c Superconducting Copper Oxides*; Springer Series in Materials Science 15; Springer-Verlag: Berlin, 1991.

(6) (a) Ikeda, N.; Hiroi, Z.; Azuma, M.; Takano, M.; Bando, Y.; Takeda, Y. *Physica C* **1993**, 210, 367–372. (b) Er, G.; Miyamoto, Y.; Kanamura, F.; Kikkawa, S. *Physica C* **1991**, *181*, 206. (c) Smith, M. G.; Manthiram, A.; Zhou, J.; Goodenough, J. B.; Markert, J. T. *Nature* **1991**, *351*, 549–551.

0897-4756/94/2806-1011$04.50/0

earth concentrations in the $La_{1-x}Sr_xCuO_y$ system.[7-10] Furthermore, high-pressure synthesis of the end member series of compounds $LaCuO_{3-\delta}$, with a wide range of oxygen stoichiometry ($0.0 \leq \delta \leq 0.5$);[11] and a rhombohedrally distorted variant with fixed composition ($LaCuO_3$)[12] has also been reported. It has also been possible to stabilize the $LaCuO_{3-\delta}$ defect perovskite phases as thin films utilizing PLD.[13] Although superconductivity has not been observed in any of the above perovskite-related compounds, a number of them exhibit mixed copper valence with good metallic characteristics.

Herein, we report on the thin-film synthesis of metastable phases in the $Sm_{1-x}Sr_xCuO_{2.5-0.5x+\delta}$ system, with x varying between 0 and 1, and δ corresponding to the excess oxygen resulting from oxidation of Cu above formal valence +2. The films are grown epitaxially on (100)-oriented $SrTiO_3$ substrates using a multitarget PLD system with *in situ* reflection high-energy diffraction (RHEED) monitoring. Prior to this work, there have been no systematic investigations of the $Sm_{1-x}Sr_xCuO_y$ ($y = 2.5-0.5x + \delta$) system in either the bulk or thin films. Aside from the doped infinite-layer phases of end member compound $SrCuO_2$, we have stabilized metastable oxygen-deficient perovskite phases over a wide range of Sm concentration. In addition, an ordered $2/\sqrt{2}a_p \times 2\sqrt{2}a_p \times a_p$ structure with mixed copper valence has been has been obtained for $x \sim 0.75$.

Experimental Details

The details of the RHEED-monitored pulsed laser deposition system have been described previously.[14,15] Briefly, the films are grown using a KrF excimer laser (248 nm), at a low deposition rate (0.05–0.1 Å/pulse), with a pulse repetition rate of 4 Hz and a fluence of 2–3 J/cm^2 at the target. The films are deposited on high-quality optically polished (100)-oriented $SrTiO_3$ substrates. The substrates are thermally attached to a heater block that can be rotated and translated for proper positioning of the azimuth and incidence angles for RHEED measurements. A computer-controlled holder assembly, which can accommodate up to six 25-mm-diameter targets, is used for mounting the ablation targets. Films with different ratios of Sm and Sr have been deposited by controlling the number of pulses used for ablation from two parent targets with compositions: $SmCuO_z$ ($z \sim 2.5$) and $SrCuO_2$. These targets are prepared by compacting and reacting mixtures of the appropriate precursor nitrates at 900–1000 °C in air. From X-ray analysis, the Sm cuprate target is observed to be a homogeneous mixture of Sm_2CuO_4 and CuO, whereas the Sr cuprate target has been determined to consist predominantly of the thermodynamically stable $SrCuO_2$ orthorhombic phase.

During deposition of the films a continuous flux of atomic O ($(1-2) \times 10^{16}$ atoms/cm^2 s), produced downstream by microwave dissociation of O_2 in a McCarrol cavity, is flowed through a quartz tube. Additionally, a pulsed source of O_2 is also directed at the substrate using an electromagnetically operated pulsed valve. The opening of the valve and the triggering of the laser are synchronized with appropriate delay to ensure that the gas jet and the ablated fragments arrive at the substrate at the same time. The continuous source of atomic O provides the necessary oxygen activity at low pressures for thermodynamic stability of the films at the growth temperature, whereas the additional high instantaneous flux of O_2 from the pulsed source supplies the oxygen required for oxidation of the large number of ablated cation species during the time of their arrival and condensation on the substrate surface.[16] The combined operation of the two sources results in a background pressure in the growth chamber of ~2 mTorr during deposition. Because of the reasonably low-pressure background, *in situ* characterization of the surface using RHEED can be easily accomplished. The pressure in the region of the RHEED gun filament is further reduced by differential pumping and is about 3 orders of magnitude lower than the pressure in the main chamber.

Prior to film deposition, the (100) $SrTiO_3$ substrates are heated to 650–700 °C and the surface cleaned using a 150-eV Ar ion beam. This is followed by homoepitaxial deposition of $SrTiO_3$, from a single-crystal $SrTiO_3$ target, until a bright and streaky RHEED pattern, with a well developed pattern of Kikuchi lines, is obtained. With additional growth of $SrTiO_3$, strong intensity oscillations of the specular spot are observed due to the two-dimensional (2D) layer-by-layer growth of the deposit.[15] The growth of the buffer layer ensures a very smooth substrate surface which is important for the growth quality of the cuprate films. Deposition of the cuprate films is normally initiated after deposition of a 100–200-Å-thick buffer layer of $SrTiO_3$.

Before growth of the $Sm_{1-x}Sr_xCuO_y$ films, a few monolayers of $SrCuO_2$ are deposited from the Sr cuprate target until a sharp and streaky RHEED pattern of the surface is observed. The $SrCuO_2$ layer provides a chemically and structurally compatible template for subsequent growth.[4] Growth of $Sm_{1-x}Sr_xCuO_y$ films with different compositions is achieved by programming the number of laser pulses used for ablation from the $SmCuO_z$ and $SrCuO_2$ targets. The deposition rates from these two targets have been observed to be quite similar. Therefore, as an example, for the growth of a film of composition Sm:Sr = 3:1, 3 pulses are used for ablation from the Sm target followed by 1 pulse from the Sr containing target in an automated sequence to complete one period. This deposition sequence is continued for about 150–200 periods, after which the growth is briefly interrupted for 30–60 s to allow time for surface recovery. The deposition–recovery cycles are repeated a number of times in a programmed mode to obtain the desired film thickness.

All of the $Sm_{1-x}Sr_xCuO_y$ films have been grown at a substrate temperature of 600 °C with a total film thickness in the range 500–750 Å. Following deposition, the films are slowly cooled down to room temperature after backfilling the chamber with 760 Torr of O_2. Some of the films have also been vacuum-annealed at the growth temperature for 30 min prior to cooldown, for which the pressure in the chamber is maintained below 10^{-5} Torr.

The cation stoichiometry of the films have been checked using EDAX and found to be within 5% of the expected values based on the programmed number of pulses used for ablation from each target. The oxygen composition of the films has, however, not been determined and is likely to vary between 2 (for $x = 1$, $\delta = 0$) and 3 (for $x = 0$, $\delta = 0.5$) as a function of film composition and annealing conditions. X-ray diffraction in the normal Bragg-reflection geometry, using Cu Kα radiation, and TEM are used for structural characterization of the films. Standard four-probe dc transport measurements have been used for electrical characterization of the films.

Results and Discussion

Structural Characterization. Our initial efforts were directed at stabilizing the end-member compound

(7) (a) Er-Rakho, L.; Michel, C.; Raveau, B. *J. Solid State Chem.* **1988**, *73*, 514–519. (b) Michel, C.; Er-Rakho, L.; Raveau, B. *J. Phys. Chem. Solids* **1988**, *49*, 451–455.

(8) (a) Tokura, Y.; Torrance, J. B.; Nazzal, A. I.; Huang, T. C.; Oritz, C. *J. Am. Chem. Soc.* **1987**, *109*, 7555–7557. (b) Murayama, N.; Sakaguchi, S.; Wakai, F.; Sudo, E.; Tsuzuki, A.; Torii, Y. *Jpn. J. Appl. Phys.* **1988**, *27*, L55–L56.

(9) De Leeuw, D. M.; Mutsaers, C. A. H. A.; Geelen, G. P. J.; Langereis, C. *J. Solid State Chem.* **1989**, *80*, 276–285.

(10) (a) Otzschi, K.; Ueda, Y. *J. Solid State Chem.* **1993**, *107*, 149–158. (b) Otzschi, K.; Hayashi, A.; Fujiwara, Y.; Ueda, Y. *J. Solid State Chem.* **1993**, *105*, 573–579.

(11) Bringley, J. F.; Scott, B. A.; La Placa, S. J.; Boehme, R. F.; Shaw, T. M.; McElfresh, M. W., Trail, S. S.; Cox, D. E. *Nature* **1990**, *347*, 263–265.

(12) (a) Demazeau, G.; Parent, C.; Pouchard, M.; Hagenmuller, P. *Mater. Res. Bull.* **1972**, *7*, 913–920. (b) Webb, A. W.; Skelton, E. F.; Qadri, S. B.; Browning, V.; Carpenter, E. R. *Phys. Rev. B* **1992**, *45*, 2480–2483.

(13) Gupta, A.; Hussey, B. W.; Guloy, A. M.; Saraf, R. F.; Bringley, J. F.; Scott, B. A. *J. Solid State Chem.* **1994**, *108*, 202–206.

(14) Chern, M. Y.; Gupta, A.; Hussey, B. W. *Appl. Phys. Lett.* **1992**, *60*, 3046–3048.

(15) Chern, M. Y.; Gupta, A.; Hussey, B. W.; Shaw, T. M. *J. Vac. Sci. Technol. A* **1993**, *11*, 637–641.

(16) Gupta, A.; Hussey, B. W.; Chern, M. Y. *Physica C* **1990**, *200*, 263–270.

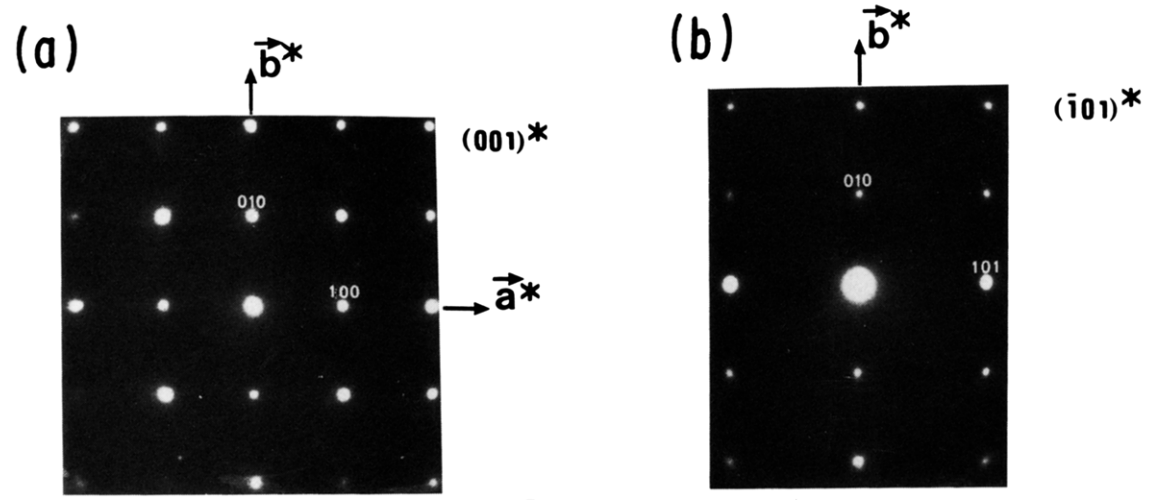

Figure 1. Electron diffraction patterns of (a) (001)* and (b) (1̄01)* planes for a $Sm_{1-x}Sr_xCuO_y$ film with $x = 0.66$. A simple perovskite-type cell, with no superstructure, is observed in the patterns.

$SmCuO_{3-\delta}$. But unlike $LaCuO_{3-\delta}$, which can be pseudomorphically stabilized as thin films,[13] it has not been possible to obtain the perovskite cuprate with Sm. The tetragonal T′ phase of Sm_2CuO_4 ($a = 3.91$ Å, $c = 11.97$ Å) is formed instead, along with separation of the excess Cu as CuO. X-ray and electron diffraction patterns of the films show that the T′ phase is very well crystallized and is oriented in a twinned arrangement with the c axis in the plane of the substrate. Although the lattice match with the substrate in the c-axis direction ($\sim 3 \times a_{SrTiO_3}$) is not as good as the match in the a–b plane, the low growth temperature tends to favor growth with the long axis in the plane of the substrate. Similar behavior has been observed for the growth of $YBa_2Cu_3O_{7-\delta}$ films.[17]

With substitution of Sr for Sm, the T′ structure is maintained for x values of up to 0.3. However, at higher concentrations a distinct perovskite-type RHEED pattern is observed during growth. Unlike the T′ (Sm_2CuO_4) phase, which exhibits a mostly spotty pattern with diffraction spots characteristic of a tripled unit cell in the c-axis direction, the RHEED pattern for the perovskite phase is sharp and streaky—comparable to that observed for $SrTiO_3$—which remains unchanged throughout the deposition process. Essentially similar patterns have been observed for $Sm_{1-x}Sr_xCuO_y$ films in the composition range $0.4 \leq x \leq 0.66$. The simple perovskite structure of these films is confirmed from their X-ray and electron diffraction patterns. The X-ray patterns for these films show only two diffraction peaks which can be indexed as the (001) and (002) reflections of the basic perovskite block. The c-axis parameter of the films has been found to vary with the Sr content and is in the range 3.85–3.70 Å. The X-ray results are discussed later in further details. Figure 1 shows electron diffraction patterns from the (001)* and (1̄01)* planes for a film with $x = 0.66$. The diffraction spots in the patterns can be indexed on the basis of an epitaxial perovskite-type phase with its a–b axes aligned with the cube axes of the substrate and $a \simeq b \sim 3.9$ Å. The diffraction from films with $x = 0.5$ and 0.4 have also been investigated and found to be similar to those shown in Figure 1. However, the spots are found to be more diffuse, particularly for the film with $x = 0.4$. Moreover, faint streaks are observed along the a^* axis and the b^* axis, possibly caused by local disorder in the crystals.

For $Sm_{1-x}Sr_xCuO_y$ films with x values in the range 0.7–0.8 an ordered structure with unit cell $2\sqrt{2}a_p \times 2\sqrt{2}a_p \times a_p$ is observed. The electron diffraction pattern of the (001)* planes for a $Sm_{1-x}Sr_xCuO_y$ film with $x = 0.75$ is shown in Figure 2a. The a_p^* and b_p^* correspond to the primitive perovskite axes, whereas the a_s^* and b_s^* correspond to the superstructure axes. The bright field image from a small region is shown in Figure 2(b). Here, the 10.9-Å periodicity along the $[110]_p^*$ and $[1\bar{1}0]_p^*$ directions is clearly observed, in agreement with the diffraction pattern in Figure 2a. Similar patterns have been observed for films with Sr compositions of $x = 0.70$ and 0.80. However, the superstructure reflections from these films are not as sharp, and weak diffusion streaks are observed in the patterns. Interestingly, when the films in this composition range are cooled in vacuum or low-pressure oxygen, instead of in 760 Torr of O_2, the diffraction patterns are more characteristic of a simple perovskite, as observed for films with $x < 0.7$.

For higher Sr concentrations, with $0.8 < x < 0.9$, a mixed-phase region is observed. The RHEED diffraction intensity from these films is quite weak and displays a complex pattern which is not easily interpreted. The electron diffraction for a film with $x = 0.85$ has been investigated and found to exhibit a perovskite-type pattern with mostly diffuse spots. Moreover, some variations in the cation composition have been observed in different regions of the sample using EDAX. The cation composition appears to be correlated with the sharpness of the reflection spots, with sharper spots being observed from Sr-rich composition regions.

Finally, for terminal Sr concentrations, $0.9 \leq x \leq 1$, the infinite-layer phase is obtained. The RHEED pattern for films in this composition range is initially streaky and slowly develops to a spotty pattern, characteristic of the tetragonal infinite-layer structure, with increasing film thickness. The presence of the infinite-layer phase is also confirmed from the X-ray and electron diffraction observations. The electron diffraction patterns for films with compositions of $x = 0.9$ and 1.0 with the incident electron beam along the c-axis are shown in parts a and b of Figure 3, respectively. The pattern for $x = 0.9$ also shows strong diffusion lines along the [100]* and [010]* directions

(17) Hamet, J. F.; Blanc-Guilhon, B.; Taffin, A.; Mercey, B.; Hervieu, M.; Raveau, B. *Physica C* **1993**, *214*, 55–63.
(18) Shannon, R. D. *Acta Crystallogr. A* **1976**, *32*, 751–767.

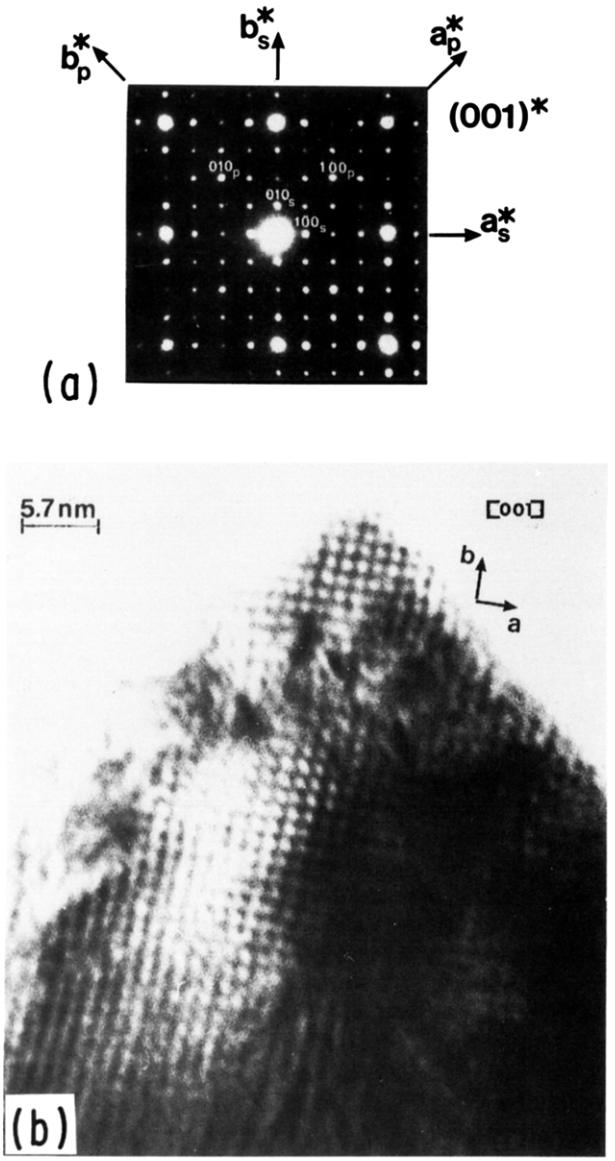

Figure 2. (a) Electron diffraction pattern of the (001)* planes for a $Sm_{1-x}Sr_xCuO_y$ film with $x = 0.75$ showing a $2\sqrt{2}a_p \times 2\sqrt{2}a_p \times a_p$ superstructure; (b) corresponding bright field image showing 10.9-Å periodicity.

suggesting the presence of randomly distributed defects in the structure.

In Figure 4 we plot the variations in the *c*-axis parameter as a function of Sr content in the $Sm_{1-x}Sr_xCuO_{2.5-0.5x+\delta}$ films for $0.4 \leq x \leq 1.0$; i.e., for samples exhibiting a perovskite-like structure. It is observed for the oxygen-annealed samples that the *c*-axis parameter decreases almost linearly with increasing x except for a small increase in the region where the ordered structure is formed. The decrease in lattice parameter on the basis of ionic size alone is unexpected since the ionic radii of Sr is larger than that of Sm.[18] Therefore, the decrease has to be attributed to a systematic decrease in the oxygen content with increasing x. It is important to point out that a small shift of the *c*-lattice parameter to lower values has been observed for films with the perovskite and ordered structures after storage for a few days. However, the original value can be restored after reannealing the films in oxygen. The decrease in lattice parameter can be attributed to a gradual loss of oxygen from the films (decrease in the δ value). The x-axis parameters for films in the Sr-rich composition range, which have been vacuum annealed prior to cooldown, are also included in Figure 4. Note that the *c*-axis lengths for these films are generally lower than those for the corresponding films which have been cooled in oxygen.

Transport Properties. Resistivity versus temperature results for $Sm_{1-x}Sr_xCuO_y$ films with varying amounts of Sr, starting with $x = 0.5$, are displayed in Figure 5. All the films have been deposited at 600 °C and then cooled under 760 Torr of O_2. If is noted that there is a progressive reduction in the room-temperature resistivity value with Sr substitution. Moreover, there is a transition from semiconducting to metallic behavior in going from the disordered perovskite phases to the ordered structure. With further increase in the Sr content the resistivity again increases rapidly and reaches the highest level for the insulating infinite-layer $SrCuO_2$ compound.

The observed results can be qualitatively interpreted based on a simple band model where the highest-energy electrons are in an antibonding σ^* band of primarily Cu 3d e_g character.[5] Because of the Cu–O bond anisotropy the degeneracy of this band will be lifted, and depending on the relative in-plane and apical Cu–O bond distances the d_{z^2} or the $d_{x^2-y^2}$ will be the highest occupied band. Furthermore, strong Coulomb correlations will split each band into two bands separated by the Hubbard gap energy U. On the basis of this simple band picture, one would expect metallic behavior for partial filling of the lower Hubbard band corresponding to mixed Cu^{2+}/Cu^{3+} valence, and insulating characteristics for complete filling with Cu^{2+}. The insulating behavior of the undoped infinite-layer phase with copper valence of +2, and the relatively low resistivity of the ordered phase with higher average Cu valence, are consistent with this model. Although the perovskite cuprates with random distribution of oxygen vacancies are also expected to have formal copper valence somewhat higher than +2, it is believed that the vacancies in these disordered structures act as efficient traps to localize the carriers, resulting in a decrease in the conductivity.

As is apparent from Figure 5, no evidence of superconductivity is observed in any of the films down to 5 K. Lack of superconductivity in the ordered compound is not surprising considering the three-dimensionality of the structure. However, phases with 2D Cu–O sheets in the structure in the composition region corresponding to Sm doping of the infinite-layer compound ($0.9 \leq x < 1$) are known to be bulk n-type superconductors.[6] The relatively high resistivity observed in Figure 5 for the $x = 0.9$ composition, with the infinite-layer-type structure, is believed to result from the presence of some excess oxygen in the doped Sr layers. Indeed, when the films are vacuum annealed instead of cooling in O_2 they exhibit a significant decrease in resistivity and show a semimetallic temperature dependence as shown in Figure 6. The removal of excess oxygen also results in a decrease in the in the *c*-axis parameter for these films as has been discussed earlier. However, the reducing conditions used so far have failed to induce superconductivity in these films. Previous efforts in obtaining superconducting infinite-layer films with Nd doping have also proved to be difficult.[19] Although the Nd-doped films are of high crystalline quality with reasonably low resistivities, they are either nonsupercon-

(19) Sugii, N.; Matsuura, K.; Kubo, K.; Yamamoto, K.; Ichikawa, M.; Yamauchi, H. *J. Appl. Phys.* **1993**, *74*, 4047–4051.

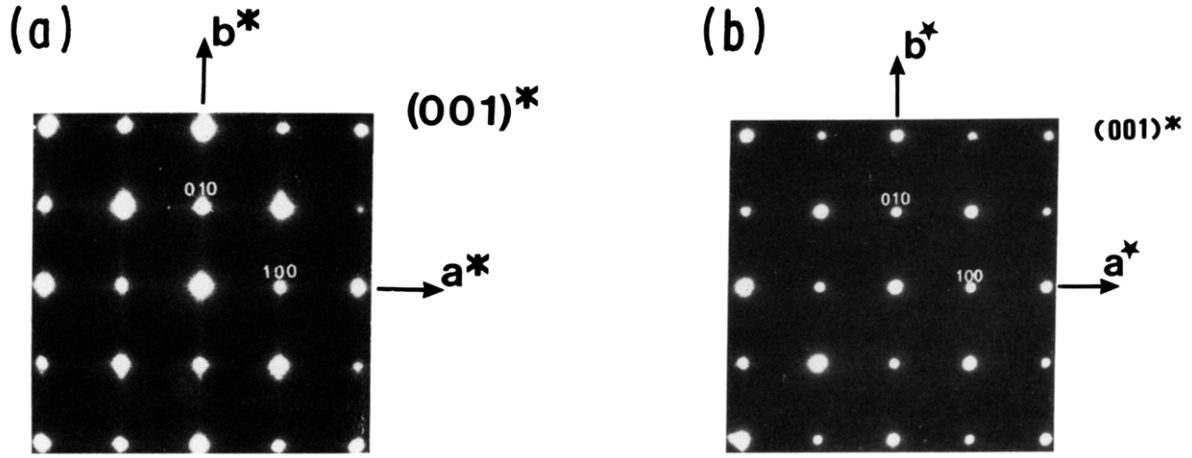

Figure 3. Electron diffraction patterns of the (001)* planes for $Sm_{1-x}Sr_xCuO_y$ films with (a) $x = 0.9$, exhibiting an infinite-layer-type structure with strong diffusion lines along the [100]* and [010]* directions; (b) $x = 1$, infinite-layer structure with no diffusion lines.

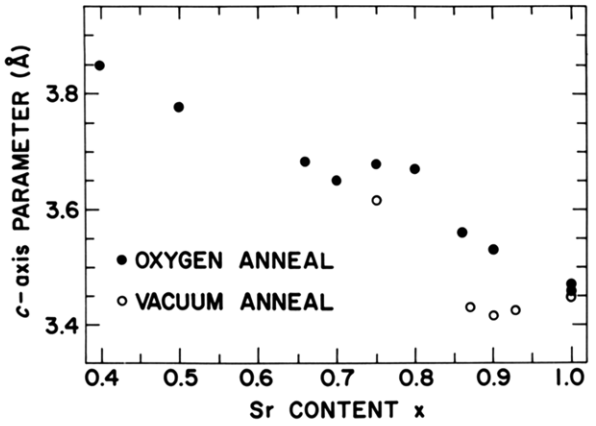

Figure 4. Plot of the c-axis lattice parameter as a function of Sr concentration in $Sm_{1-x}Sr_xCuO_y$ films. The solid circles refer to films cooled in 760 Torr of O_2, whereas open circles are for films which are vacuum annealed prior to cooldown.

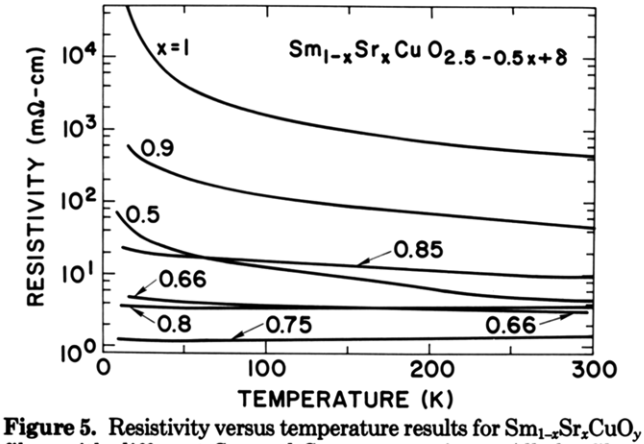

Figure 5. Resistivity versus temperature results for $Sm_{1-x}Sr_xCuO_y$ films with different Sm and Sr concentrations. All the films have been grown at 600 °C under the same oxidation conditions and subsequently cooled under 760 Torr of O_2.

ducting or show a very broad superconducting transition. It has been suggested that incomplete relaxation of the lattice mismatch between the film and the substrate, or the presence of intergrowth regions which locally cause cation deficiency at the Sr(Nd) site, may be responsible for this behavior.[19] Finally we note that, in contrast to the behavior of the infinite-layer composition with mixed Cu^+/Cu^{2+} valence, the $x = 0.75$ compsition film with the ordered structure actually shows an increase in resistivity when it is vacuum annealed, as seen in Figure 6. This is

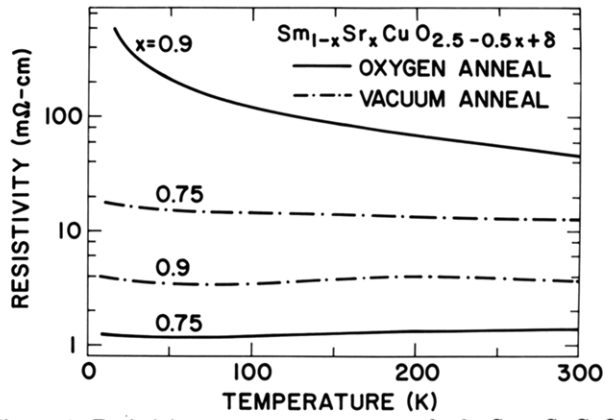

Figure 6. Resistivity versus temperature results for $Sm_{1-x}Sr_xCuO_y$ films with $x = 0.75$ and 0.9 under different annealing conditions. Dashed lines correspond to films which have been cooled in O_2 (same as in Figure 5), whereas dot–dashed lines correspond to films which have been vacuum annealed at the growth temperature for 30 min prior to cooldown.

likely caused by a reduction in the formal Cu valence to a value closer to +2 due to removal of oxygen from the structure.

Concluding Remarks

From the above results it is clear that a large homogeneity range of perovskite-type phases exists in the $Sm_{1-x}Sr_xCuO_y$ system. The existence of extra spots and diffuse streaks in the electron diffraction patterns as a function of cation composition, however, suggests that complex ordering phenomena and non-stoichiometric features are prevalent in the perovskite matrix. They could originate in different sizes and coordination of Sm and Sr cations and/or the oxygen vacancy distribution. The following summarizes some of the general features of the observed structural evolution in the $Sm_{1-x}Sr_xCuO_y$ system:

(a) Unlike the the La-based cuprates, no perovskite phases have been stabilized for $x = 0$.

(b) The stabilization of a perovskite-like structures is only achieved with strontium substitution ($0.4 \leq x \leq 0.66$). In this composition range oxygen-deficient perovskites are observed with possibly random distribution of the vacancies. Taking into consideration the general composition of the phase, $Sm_{1-x}Sr_xCuO_{2.5-0.5x+\delta}$, which expresses the oxygen content results for both Sm^{3+}/Sr^{2+} substitution ($-0.5x$) and Cu^{2+}/Cu^{3+} oxidation ($+\delta$), the defect perovskite

composition varies from $Sm_{0.6}Sr_{0.4}CuO_{2.30+\delta}$ to $Sm_{0.34}Sr_{0.66}CuO_{2.17+\delta}$.

(c) In a narrow composition region near $x \sim 0.75$ an ordered $2\sqrt{2}a_p \times 2\sqrt{2}a_p \times a_p$ structure is observed which exhibits metallic behavior. The structural details of this phase are presently being investigated using high-resolution electron microscopy and will be reported elsewhere.

(d) For the substitution range near the terminal $SrCuO_2$ composition ($0.9 \leq x \leq 1$), the infinite-layer-type structure is stabilized. This structure can be derived from the perovskite ABO_3 structure by simply removing the oxygen atoms from the AO layer, leading to an 8-fold-coordination for A cations and 4-fold-coordination for the B cations. It is believed that under oxidizing conditions, a small amount of oxygen is introduced into the A-site layers with Sm substitution leading to localization of carriers. A significant decrease in the resistivity of the films has been observed after vacuum annealing, possibly from removal of the excess oxygen.

Acknowledgment. We thank A. M. Guloy and P. R. Duncombe for preparation of the ablation targets. We are also grateful to B. A. Scott for useful discussions and suggestions.